Mechanism of Olefin Metathesis with Catalysis by Ruthenium Carbene Complexes: Density Functional Studies on Model Systems

Sergei F. Vyboishchikov, Michael Bühl, and Walter Thiel*[a]

Abstract: Gradient-corrected (BP86) density functional calculations were used to study alternative mechanisms of the metathesis reactions between ethene and model catalysts $[(PH_3)(L)Cl_2Ru{=}CH_2]$ with $L = PH_3$ (**I**) and $L = C_3N_2H_4$ = imidazol-2-ylidene (**II**). On the associative pathway, the initial addition of ethene is calculated to be rate-determining for both catalysts ($\Delta G^{\ddagger}_{298} \approx 22-25$ kcal mol^{-1}). The dissociative pathway starts with the dissociation of phosphane, which is rather facile ($\Delta G^{\ddagger}_{298} \approx 5-10$ kcal mol^{-1}). The resulting active species $(L)Cl_2Ru{=}CH_2$ can coordinate ethene *cis* or *trans* to L. The *cis* addition is unfavorable and mechanistically irrelevant ($\Delta G^{\ddagger}_{298} \approx 21-25$ kcal mol^{-1}). The *trans* coordination is barrierless, and the rate-determining step in the subsequent catalytic cycle is either ring closure of the π complex to yield the ruthenacyclobutane (catalyst **I**, $\Delta G^{\ddagger}_{298} = 12$ kcal mol^{-1}), or the reverse reaction (catalyst **II**, ring opening, $\Delta G^{\ddagger}_{298} = 10$ kcal mol^{-1}), that is, **II** is slightly more active than **I**. For both catalysts, the dissociative mechanism with *trans* olefin coordination is favored. The relative energies of the species on this pathway can be tuned by ligand variation, as seen in $(PMe_3)_2Cl_2Ru{=}CH_2$ (**III**), in which phosphane dissociation is impeded and olefin insertion is facilitated relative to **I**. The differences in calculated relative energies for the model catalysts **I**–**III** can be rationalized in terms of electronic effects. Comparisons with experiment indicate that steric effects must also be considered for real catalysts containing bulky substituents.

Keywords: density functional calculations · metathesis · reaction mechanisms · ruthenium · transition states

Introduction

Olefin metathesis is a powerful method for the formation of carbon–carbon double bonds[1–4] which is used extensively in organic synthesis. Applications include ring-opening metathesis polymerization (ROMP), ring-closing metathesis (RCM), ring-opening metathesis (ROM), acyclic diene metathesis polymerization (ADMET), and cross-metathesis (CM). Over the past decade, well-defined ruthenium-based catalysts have been developed which combine high activity and excellent tolerance to many common functional groups.[1–4] Grubbs et al. introduced the first such catalysts with the general formula $[(PR_3)_2X_2Ru{=}CHR']$,[5] the most prominent example being $[(PCy_3)_2Cl_2Ru{=}CHPh]$.[6] These complexes are pentacoordinate and have a distorted square-pyramidal geometry with the alkylidene in the axial position and the *trans* phosphanes and halides in the equatorial plane.[6] The replacement of one trialkylphosphane ligand by an N-heterocyclic carbene (NHC)[7] has led to a new class of metathesis catalysts with the general formula $[(PR_3)(NHC)X_2Ru{=}CHR']$[8–10] which are even more active than the original Grubbs complexes. Ruthenium carbene complexes with chelating bis(phosphane) ligands, and hence *cis* stereochemistry, also act as catalysts for olefin metathesis, particularly in their cationic forms.[11]

The generally accepted Chauvin mechanism[12] of metathesis reactions consists of a series of formal $[2+2]$ cycloadditions and cycloreversions (Scheme 1). It involves olefin coordination to the transition metal carbene complex to form a π complex, migratory insertion of the olefin ligand into the metal–carbene bond to yield a metallacyclobutane, breaking two different bonds in the metallacyclobutane to form another π complex, and dissociation to give the products. In a degenerate metathesis reaction, the last two steps are the exact reverse of the first two steps.

Although there is concensus on these general mechanistic features, the detailed course of metathesis reactions depends on the chosen catalyst. Consequently, the mechanism of olefin metathesis with catalysis by ruthenium carbene complexes has been the subject of intense experimental studies.[13–23] These include systematic kinetic measurements in solution[13–17] and in the gas phase by electrospray ionization tandem mass spectrometry (ESI-MS/MS),[18–21] as well as the determination

[a] Prof. Dr. W. Thiel, Dr. S. F. Vyboishchikov, Dr. M. Bühl
Max-Planck-Institut für Kohlenforschung
Kaiser-Wilhelm-Platz 1, 45470 Mülheim/Ruhr (Germany)
Fax: (+49) 208-306-2996
E-mail: thiel@mpi-muelheim.mpg.de

Supporting information for this article is available on the WWW under http://www.chemeurj.org/ or from the author.

  0947-6539/02/0817-3962 $ 20.00+.50/0

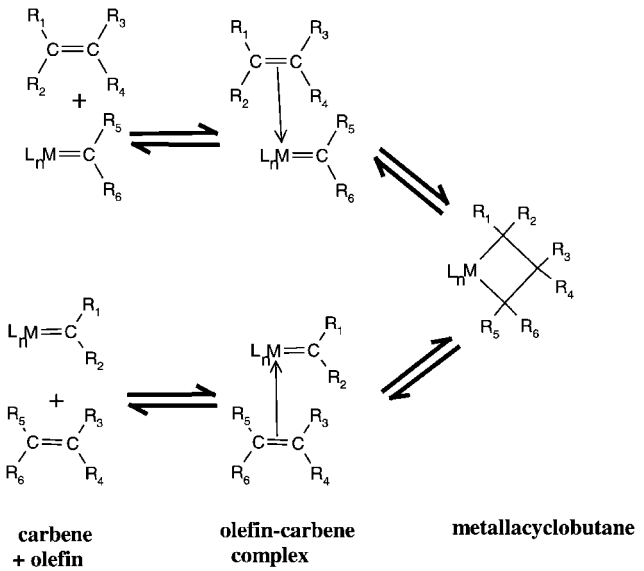

Scheme 1. General mechanism of transition metal catalyzed olefin metathesis (generalized Hérisson–Chauvin mechanism).

of X-ray structures for complexes related to possible intermediates.[11c, 22, 23] These studies have resolved a number of mechanistic issues, while others are still open.

There are two basic pathways for catalysis by ruthenium carbene complexes of the type $[(PR_3)(L)X_2Ru{=}CHR']$ (L = PR_3, NHC; X = halide): The associative mechanism (see Scheme 2) assumes the initial addition of the olefin to yield a hexacoordinate, octahedral 18-electron complex, while the dissociative mechanism (see Scheme 3) starts with the dissociation of one phosphane ligand to form a tetracoordinate 14-electron complex. Early mechanistic work in solution[4, 13, 14] suggested an associative path on the basis of a preference for the 18-electron over the 14-electron intermediate, and established phosphane dissociation as a critical step along the reaction coordinate, while the most recent investigations[16, 17] clearly favor the dissociative path. The tetracoordinate 14-electron intermediates were unambiguously identified by gas-phase ESI-MS/MS studies both for Grubbs-type catalysts with a cationized phosphane ligand[18–20] and for cationic Hofmann-type catalysts.[20–21] Hence, the recent experimental evidence[16–21, 23] clearly supports a dissociative mechanism via a tetracoordinate intermediate $[(L)X_2Ru{=}CHR']$ (L = PR_3, NHC; X = halide).

The addition of olefin to this intermediate may occur *cis* or *trans* to the ligand L. Both approaches are considered in experimental papers, and the proposed reaction schemes show both *cis*[3, 4, 13, 14] and *trans*[4, 13, 19, 20] olefin coordination. The most recent work in solution does not indicate the stereochemistry about the ruthenium center during the catalytic cycle because of the lack of reliable experimental evidence.[17] Similarly, it is experimentally not yet clear[17] whether the metallacyclobutane is actually an intermediate (as drawn in the Chauvin mechanism, see Scheme 1) or merely a transition state. In fact, the latter possibility was recently favored on the basis of electronic substituent effects and kinetic isotope effects observed in gas-phase mechanistic studies, although alternative interpretations could not be wholly ruled out.[19] From an experimental point of view, there is still considerable uncertainty about the details of the catalytic cycle.

The current mechanistic picture of catalysis by ruthenium carbene complexes of the type $[(PR_3)(L)X_2Ru{=}CHR']$ involves an initiation phase (dissociation of PR_3) and subsequent metathesis reaction with the olefin (catalytic cycle). For the active tetracoordinate species $[(L)X_2Ru{=}CHR']$, there is competition between olefin coordination (leading to metathesis) and recombination with free PR_3 (deactivation). The relative rates of these processes depend on the chosen catalyst.[16, 17, 20, 21] To be more specific, the experimentally studied Grubbs-type complexes with L = PR_3 initiate more easily than those with L = NHC, while the latter are more active in the catalytic cycle and less prone to deactivation;[16, 17] the Hofmann-type catalysts[11] initiate most easily, but their intrinsic metathesis rates in the gas phase are somewhat lower.[20] The variation of the ligands and substituents (L, X, R, R′) in the complexes $[(PR_3)(L)X_2Ru{=}CHR']$ has a significant impact on initiation rates and on catalyst activity towards different substrates in solution,[17] and efficient catalyst screening is therefore highly desirable.[21, 24, 25]

Theoretical studies of olefin metathesis may be useful to gain deeper mechanistic insights, especially with regard to issues that have not yet been resolved experimentally (see above). Topics of interest are the characterization of all intermediates and transition states in the catalytic cycle, the stereochemistry including possible conformational changes during the reaction, the identification of the rate-determining steps, the differences between different catalysts, and the selectivity toward different substrates. Given the importance of olefin metathesis reactions with Ru-based catalysts, surprisingly little theoretical work has been reported in the literature. There are early computational studies on titanium-catalyzed metathesis.[26] More recent work on high-valent molybdenum alkylidene catalysts[27–29] addressed their electronic structure,[27] the conformations, stability, and formation of the corresponding metallacyclobutane,[28] as well as the rotational barrier for the carbene ligand and the *syn*/*anti* stereochemistry.[29] Concerning ruthenium carbene complexes, Car–Parrinello molecular dynamics simulations were used to study the behavior of the model compound $[(PH_3)_2Cl_2Ru{=}CH_2]$ and its reaction with ethene at several temperatures between 300 K and 1273 K:[30] for $[(PH_3)_2Cl_2Ru{=}CH_2]$, strong structural fluctuations were seen (including *cis*/*trans* isomerization of the Cl ligands and rotation around the $Ru{=}CH_2$ bond) which culminated in the loss of one PH_3 ligand at 1273 K after 600 fs, and the approach of ethene to $[(PH_3)_2Cl_2Ru{=}CH_2]$ was found to result in insertion to give the ruthenacyclobutane and even complete metathesis for a suitably prepared simulation system under certain conditions.[30] In addition, some recent experimental studies on ruthenium carbene complexes were accompanied by theoretical calculations[10a, 11, 19] which focused on the Ru–ligand bond strengths in $[(PR_3)(L)Cl_2Ru{=}CH_2]$ (R = H, Me; L = PR_3, NHC),[10a] on the structure and stability of model compounds for Hofmann-type catalysts,[11] and on the dissociative path for the reaction between $[(PH_3)_2Cl_2Ru{=}CH_2]$

  0947-6539/02/0817-3963 $ 20.00+.50/0

and ethene.[19] Finally, there is unpublished theoretical work on the reactions between the fully substituted catalysts [$(PCy_3)(L)Cl_2Ru{=}CHPh$] and ethene.[31]

Our theoretical interest in the mechanism of ruthenium-catalyzed metathesis reactions was triggered by surprising stereochemical observations made in the RCM step of the total synthesis of (−)-salicylihalamide.[32] In the first stage of a corresponding computational investigation, we have studied both the associative and dissociative mechanisms of the metathesis reactions involving ethene and several model catalysts (focusing on [$(PH_3)_2Cl_2Ru{=}CH_2$] and [$(PH_3)(NHC)Cl_2Ru{=}CH_2$] with NHC = $C_3N_2H_4$). Herein we describe the results from these model calculations, in order to provide a firm basis for the computational studies on the complete system,[32] which will be reported elsewhere.

Methods of Calculation

The quantum-chemical calculations were carried out with density functional theory (DFT).[33, 34] They employed the gradient-corrected BP86 functional, which combines the Becke exchange[35] and Perdew correlation[36] functionals. For ruthenium we used a small-core, quasirelativistic effective core potential with the associate (7s6p5d)/[5s3p3d] valence basis set contracted according to a (31111/411/311) scheme.[37] The other elements were represented by the 6-31G(d) basis[38] with one set of d polarization functions at all non-hydrogen atoms. Spherical d functions were used throughout.

Geometries were optimized without any constraints. Minima and transition states were first approximately located with the TURBOMOLE package[39] to take advantage of the efficient RI-DFT approach[40] and then refined with Gaussian 98.[41] The optimized stationary points were characterized as minima or transition states by analytic computation of the harmonic force constants with Gaussian 98.[41] All numerical results reported were taken from Gaussian 98 and thus refer to its BP86 implementation. Zero-point vibrational energies were calculated by using the harmonic approximation, and thermodynamic properties were evaluated within the harmonic oscillator/rigid rotator approximation as implemented in Gaussian 98.

For transition metal compounds, the chosen DFT approach (BP86 functional with medium-size basis sets) normally provides realistic geometries, relative energies, and vibrational frequencies [34, 42–45]. For further validation, we performed additional B3LYP[46, 47] and CCSD(T)[48, 49] calculations for some of the systems studied here, using the same basis sets and effective core potentials as in BP86. The computations with the B3LYP hybrid functional involved full geometry optimizations, while the coupled cluster CCSD(T) calculations were performed on the BP86 geometries with the MOLPRO program package.[50] Generally, the B3LYP and CCSD(T) results are in good agreement with the BP86 results (for details, see below) and thus validate the use of the BP86 functional in the current study.

Results

Model systems and notation: We investigated metathesis reactions involving ethene and several model catalysts [$(PR_3)(L)Cl_2Ru{=}CHR'$]. Most of the calculations focused on the complexes [$(PH_3)(L)Cl_2Ru{=}CH_2$] with L = PH_3 (**I**) and L = NHC = $C_3N_2H_4$ (**II** containing an imidazol-2-ylidene ligand). For comparison, some additional calculations were performed for [$(PMe_3)_2Cl_2Ru{=}CH_2$] (**III**).

The overall metathesis reactions between ethene and catalysts **I**–**III** are degenerate. It is therefore sufficient to follow these reactions only up to the metallacycle (see Scheme 2 and Scheme 3) since the subsequent steps are then simply the reverse of the preceding steps. For the associative mechanism (Scheme 2) we need consider only the addition of the ethene to the catalyst [$(PH_3)(L)Cl_2Ru{=}CH_2$] (**1**) to form the corresponding π complex (conformations **2** and **3**) and the following insertion to give the metallacycle **4**. In the case of the dissociative mechanism (Scheme 3), we need only study the initial loss of PH_3 to yield [$(L)Cl_2Ru{=}CH_2$] (**5**) and the subsequent addition/insertion reactions of ethene via the π

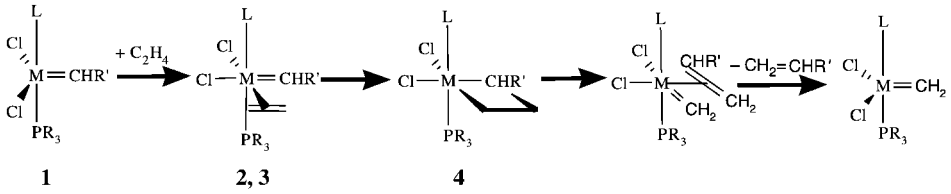

Scheme 2. Associative mechanism of olefin metathesis with [$(PR_3)(L)Cl_2Ru{=}CHR'$] catalysts. The labels are used in the text for R = R′ = H.

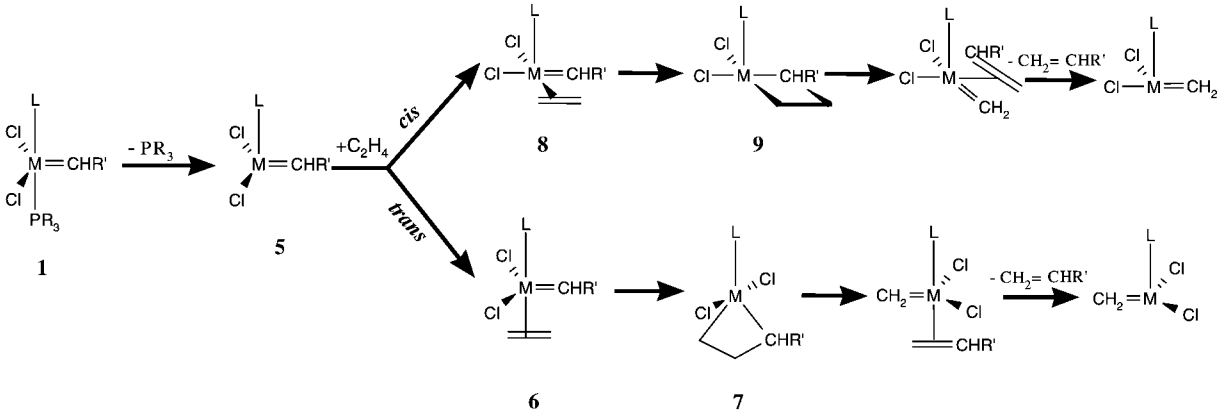

Scheme 3. Dissociative mechanism of olefin metathesis with [$(PR_3)(L)Cl_2Ru{=}CHR'$] catalysts (*cis* and *trans* pathways). The labels are used in the text for R = R′ = H.

0947-6539/02/0817-3964 $ 20.00+.50/0 *Chem. Eur. J.* **2002**, *8*, No. 17

complex to give the metallacycle (*trans*: **5** → **6** → **7**; *cis*: **5** → **8** → **9**). The generic labels **1**–**9** are associated with a given catalyst by a corresponding prefix (e.g., **I-1**), and transition states are denoted analogously (e.g., **I-TS12** refers to the conversion of **I-1** to **I-2**).

The energetics of metathesis reactions are presented in terms of relative energies at 0 K including zero-point vibrational corrections (ΔE_0), enthalpies at 298 K (ΔH°_{298}), and Gibbs free energies at 298 K (ΔG°_{298}). The text and the figures normally refer to ΔE_0, but ΔG°_{298} is also discussed if required. The underlying quantum-chemical results are documented in the Supporting Information.

Associative mechanism: Figure 1 and Figure 2 depict the relevant stationary points of the associative metathesis pathway for catalysts **I** and **II**, respectively. Figure 3 and Figure 4 show the corresponding potential energy profiles.

The first step of the associative mechanism is the coordination of ethene to the metal atom, which must occur *cis* to the methylidene ligand to allow for the subsequent insertion. The transition states for ethene coordination (**I-TS12**, **II-TS12**) are rather loose, with Ru–C distances of more than 3 Å and a fairly undistorted ethene moiety, but there are significant geometrical changes in the ligand sphere, particularly for the Cl-Ru-Cl angle (reactants: **I-1** 142.7°, **II-1** 147.2°; transition states: **I-TS12** 110.2°, **II-TS12** 111.5°). The energetic consequences of the distortions can be quantified by the reorganization energy of the $[(PH_3)(L)Cl_2Ru{=}CH_2]$ fragments (i.e., the difference of its total energy at the geometry in the transition state and in the fully optimized reactant). The values of 11.7 (**I**) and 14.4 kcal mol^{-1} (**II**) are quite close to the calculated barriers of 12.8 (**I**) and 14.9 kcal mol^{-1} (**II**), that is, these barriers are largely caused by distortions within the metal complex. As in any associative process, the entropic contributions raise the free energy barrier $\Delta G^{\pm}_{298}$ further, and lead to values of 22.1 and 25.0 kcal mol^{-1} for **I** and **II**, respectively.

The π complexes formed upon coordination of ethene are distorted octahedra, with Cl-Ru-Cl angles of about 95°. In the lowest energy conformation (**I-2**, **II-2**) the C=C bond of the ethene ligand is perpendicular to the equatorial plane defined by Cl-Ru-Cl and contains the carbene ligand CH_2 (see Figure 1 and Figure 2). Internal rotation of the carbene ligand about the Ru=C bond is facile and requires only 1.7 kcal mol^{-1} in **I-2** and 3.5 kcal mol^{-1} in **II-2**.

The intrinsic interaction energies between ethene and the metal moiety in the π complex are quite high (e.g., −47.7 kcal mol^{-1} in **I-2**), but they are largely compensated by the reorganization energies between the ethene and metal moieties in the π complex that are needed to distort their geometries (e.g., 30.9 kcal mol^{-1} for **I-1** and 11.2 kcal mol^{-1} for ethene). Hence, the formation of the π complexes only leads to a small net stabilization ($\Delta E_0 = -5.6$ kcal mol^{-1} in **I-2**, −4.8 kcal mol^{-1} in **II-2**) and is even endoergic at room temperature ($\Delta G^\circ_{298} = 5.3$ kcal mol^{-1} for **I-2**, 6.7 kcal mol^{-1} for **II-2**) due to the entropic contribution. For the insertion reaction to occur, the olefin and carbene ligands must lie in the same plane. Starting from the lowest energy "perpendicular" conformer of the π complex **2**, internal rotation of the ethene moiety leads to such a "coplanar" conformer **3** via a transition state **TS23** which is energetically and geometrically very similar to **3**. The "coplanar" conformer is less stable than the "perpendicular" conformer by 6 kcal mol^{-1}. An analysis of the corresponding frontier orbitals shows that both conformations should be similarly well suited for σ donation and π backdonation, and the difference in stability is therefore of steric origin.

To initiate ring closure of the π complex **3** to form the ruthenacycle **4**, the methylidene ligand must rotate out of the equatorial plane (see Figure 1 and Figure 2). In the corresponding transition state **TS34**, this internal rotation has essentially been completed, but the new C–C bond is not yet formed: the corresponding C carbene ··· C olefin distance is still large (2.41 Å in **I-TS34**, 2.37 Å in **II-TS34**), and the ethene

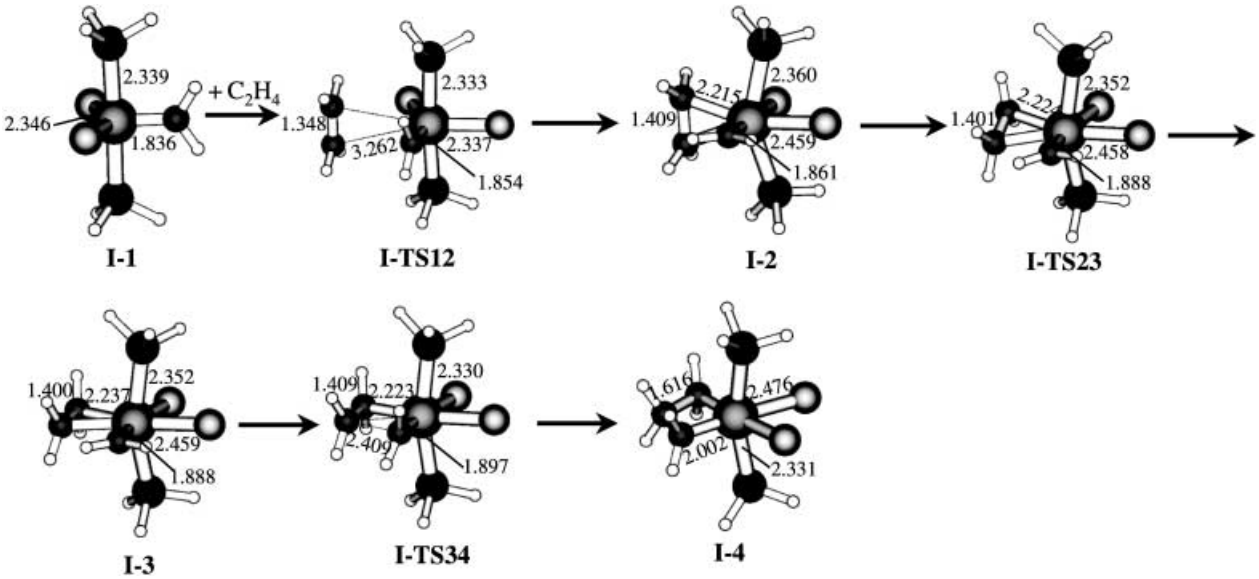

Figure 1. Associative mechanism of ethene metathesis for the $[(PH_3)_2Cl_2Ru{=}CH_2]$ catalyst (**I**). Bond lengths are given in Å. Transition states are denoted by TS.

  0947-6539/02/0817-3965 $ 20.00+.50/0

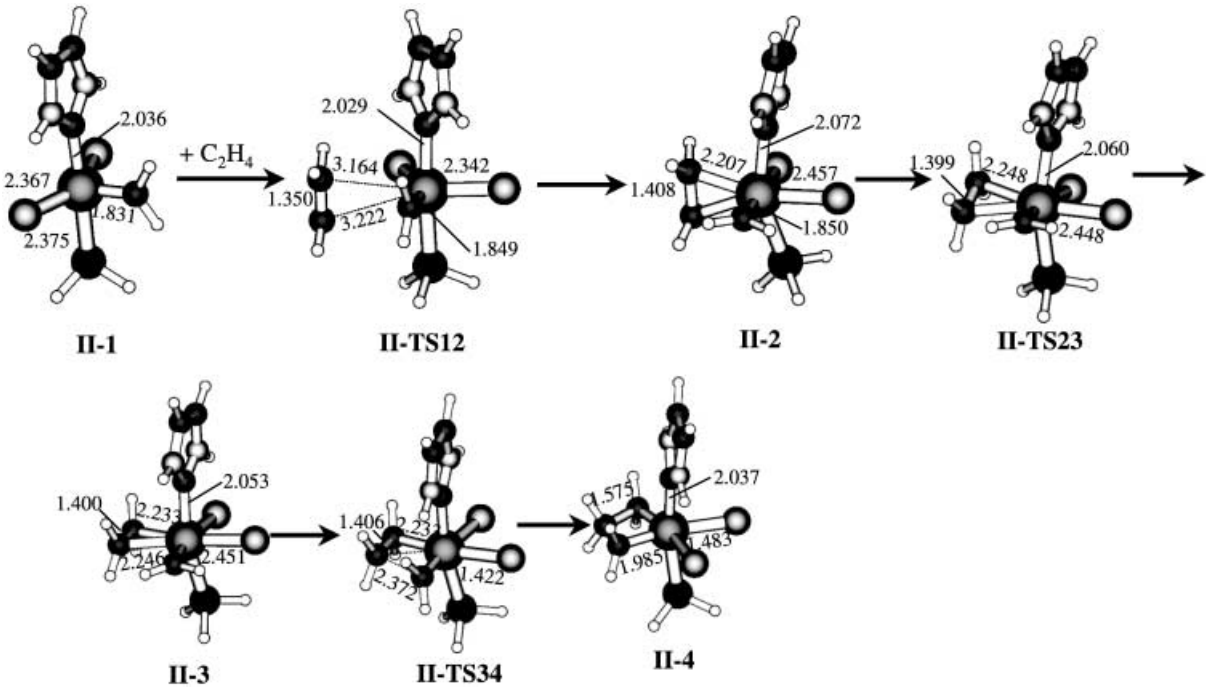

Figure 2. Associative mechanism of ethene metathesis for the $[Cl_2(PH_3)(C_3N_2H_4)Ru{=}CH_2]$ catalyst (**II**). Bond lengths are given in Å. Transition states are denoted by TS.

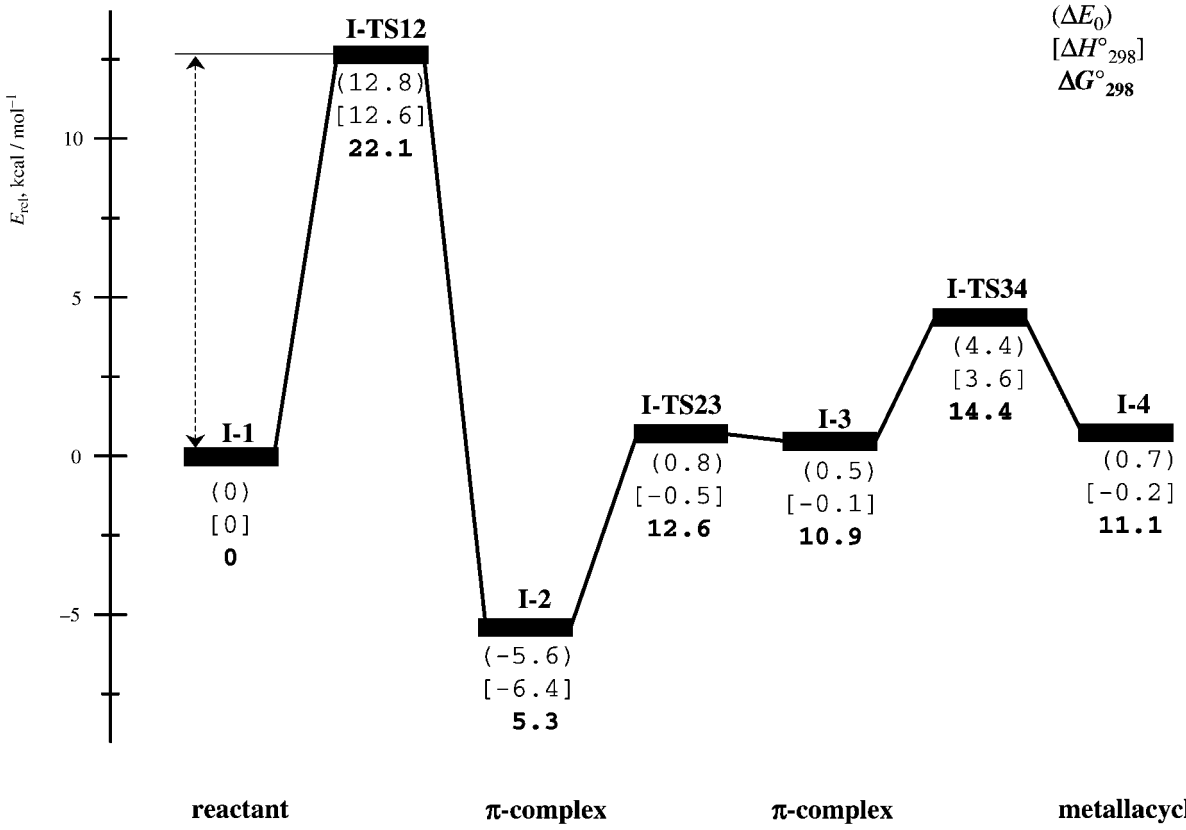

Figure 3. Potential energy profile of ethene metathesis for the associative mechanism with the $[(PH_3)_2Cl_2Ru{=}CH_2]$ catalyst (**I**). Values in parentheses indicate the relative energies at 0 K (ΔE_0), those in square brackets are enthalpies at 298 K (ΔH°_{298}), and bold values without brackets are Gibbs free energies at 298 K (ΔG°_{298}). The depicted energy levels refer to ΔE_0. The rate-determining step is marked by an arrow.

0947-6539/02/0817-3966 $ 20.00+.50/0 *Chem. Eur. J.* **2002**, *8*, No. 17

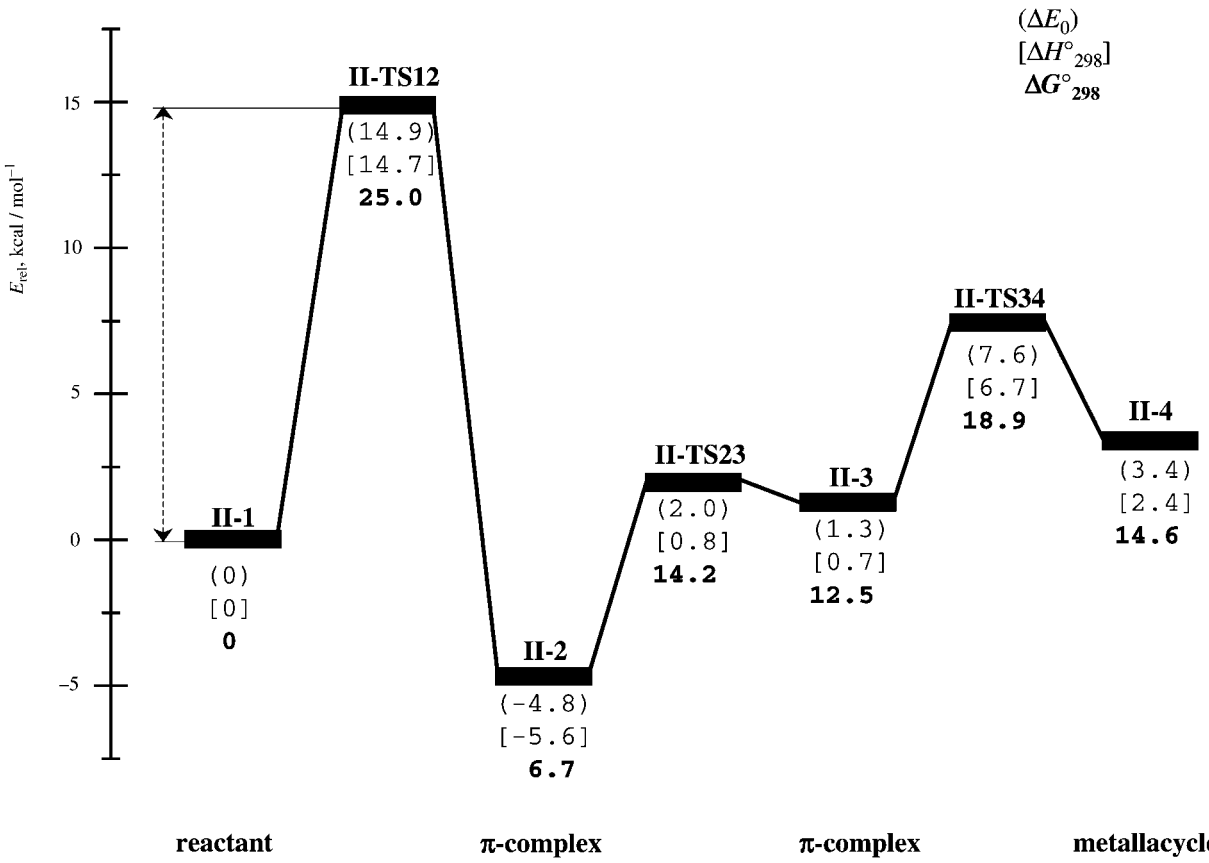

Figure 4. Potential energy profile of ethene metathesis for the associative mechanism with the [$Cl_2(PH_3)(C_3N_2H_4)Ru{=}CH_2$] catalyst (**II**). The notations are the same as in Figure 3.

C=C bond is only slightly elongated (by less than 0.01 Å relative to **3**). Hence, **TS34** is an early transition state with regard to C–C bond formation. The barrier for ethene insertion **3** → **4** is quite small for both catalysts (3.9 and 6.3 kcal mol^{-1} for **I** and **II**, respectively). Likewise, the reverse ring opening reaction of the ruthenacycle **4** is also very facile, with calculated barriers of 3.7 (**I**) and 4.2 kcal mol^{-1} (**II**).

In summary, the reactions of the associative pathway proceed in a very similar manner for both catalysts. The initial olefin coordination is the rate-determining step in each case. The corresponding barrier is somewhat higher for catalyst **II** than for catalyst **I** ($\Delta G^{\ddagger}_{298}$: 25 versus 22 kcal mol^{-1}). The subsequent internal rotation and insertion of the olefin require less activation, with barriers of less than 8 kcal mol^{-1} (again slightly higher for **II**).

Dissociative mechanism: Figure 5, Figure 6, Figure 7, and Figure 8 show the relevant stationary points of the dissociative metathesis pathway for both *trans* and *cis* coordination of the olefin to the intermediate arising from catalysts **I** and **II**, respectively. Figure 9 and Figure 10 compare the resulting potential energy profiles.

The initial dissociation of PH_3 from [$(PH_3)(L)Cl_2Ru{=}CH_2$] (**1**) yields the tetracoordinate species [$(L)Cl_2Ru{=}CH_2$] (**5**),

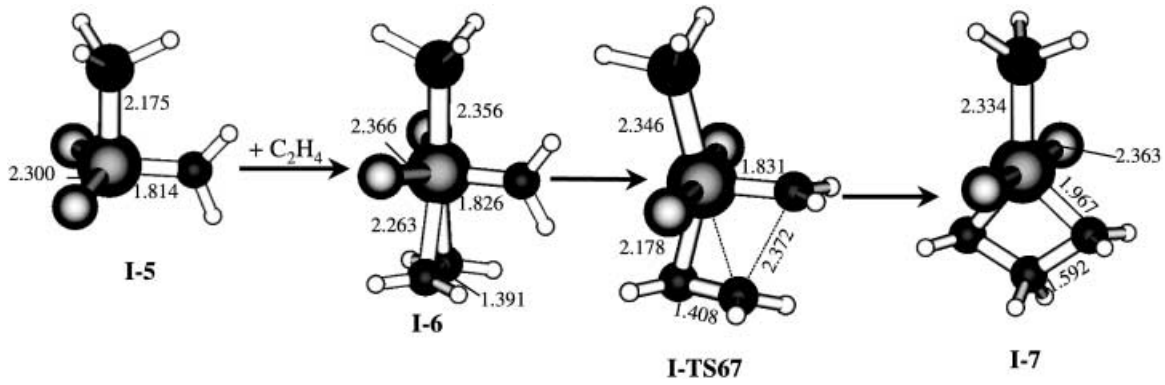

Figure 5. Dissociative mechanism of ethene metathesis with the [$(PH_3)_2Cl_2Ru{=}CH_2$] catalyst (**I**) (*trans* olefin coordination). Bond lengths are given in Å. Transition states are labeled TS.

  0947-6539/02/0817-3967 $ 20.00+.50/0

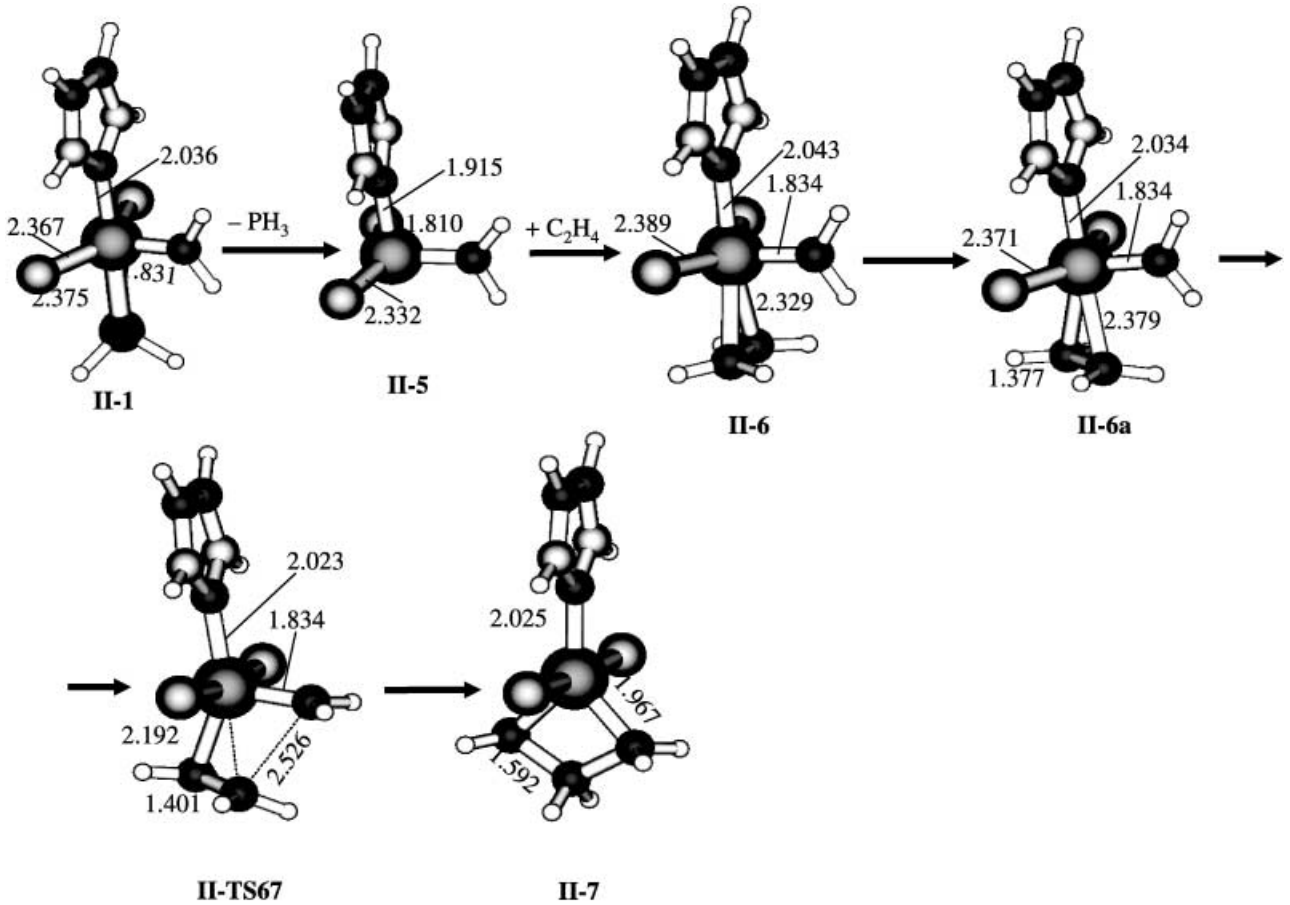

Figure 6. Dissociative mechanism of ethene metathesis with the $[Cl_2(PH_3)(C_3N_2H_4)Ru{=}CH_2]$ catalyst (**II**) (*trans* olefin coordination). Bond lengths are given in Å. Transition states are labeled TS.

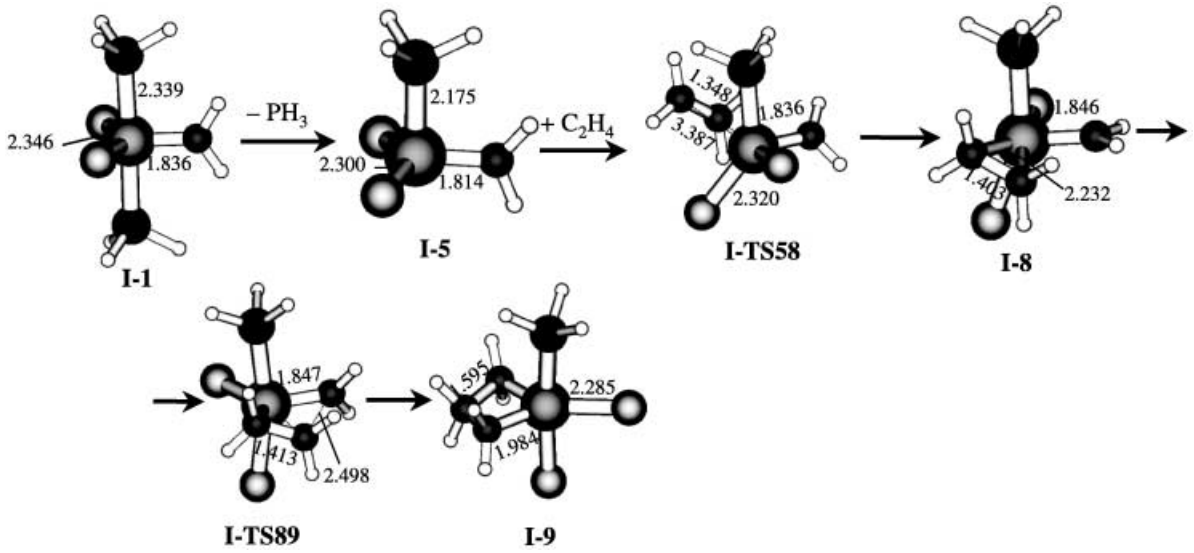

Figure 7. Dissociative mechanism of ethene metathesis with the $[(PH_3)_2Cl_2Ru{=}CH_2]$ catalyst (**I**) (*cis* olefin coordination). Bond lengths are given in Å. Transition states are labeled TS.

which acts as the active catalyst. With respect to its overall shape, **5** resembles the corresponding fragment in **1**; the bond angles are similar, while the bond lengths involving Ru are shortened, particularly for Ru–L (Ru–P in **I-5** by 0.18 Å, Ru–C in **II-5** by 0.12 Å). The dissociation **1** → **5** proceeds uphill on the potential energy surface, without an intervening transition state. It is endothermic by 20.2 kcal mol^{-1} for catalyst **I** and by 17.2 kcal mol^{-1} for catalyst **II** in terms of ΔE_0. Including entropic effects (ΔG°_{298}) reduces these values to 9.4 and 5.8 kcal mol^{-1}, respectively. The Arduengo-type carbene ligand in **II** (L = $C_3N_2H_4$, imidazol-2-ylidene) is known to be a stronger σ donor than the phosphane ligand

0947-6539/02/0817-3968 $ 20.00+.50/0 *Chem. Eur. J.* **2002**, *8*, No. 17

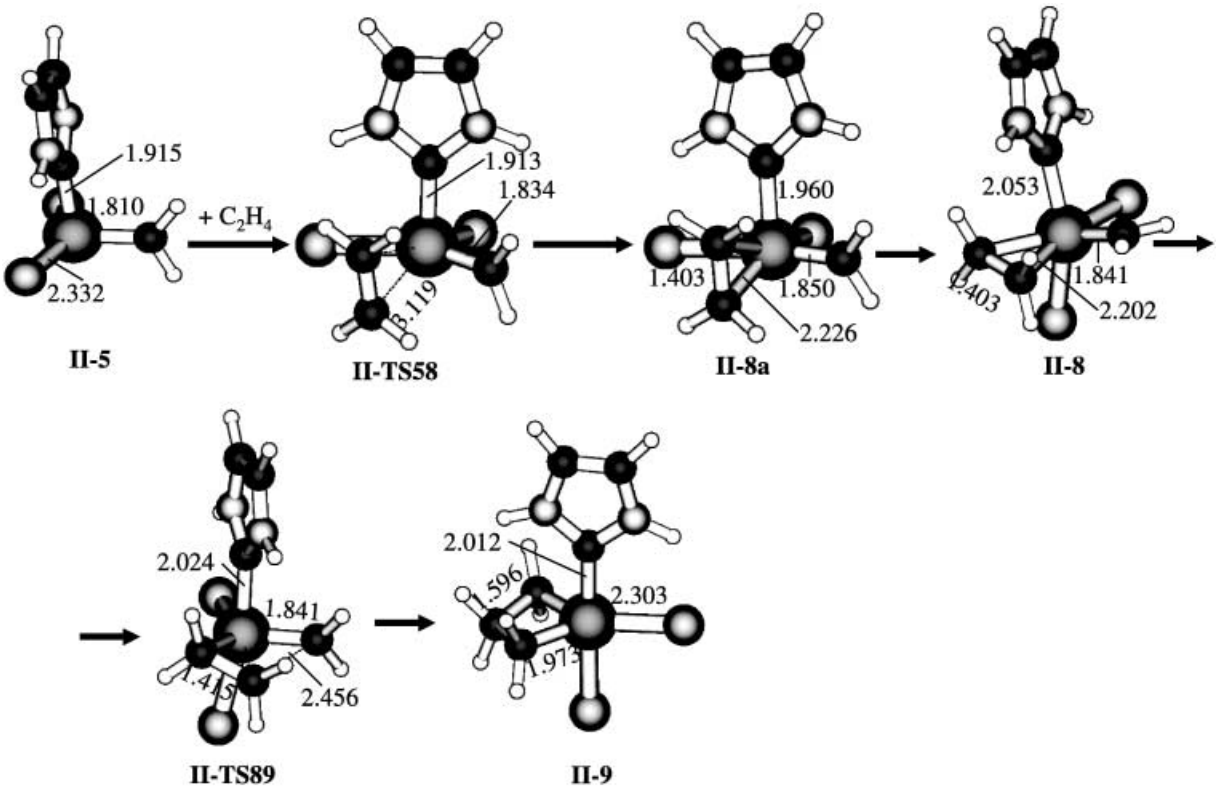

Figure 8. Dissociative mechanism of ethene metathesis with the $[Cl_2(PH_3)(C_3N_2H_4)Ru{=}CH_2]$ catalyst (**II**) (*cis* olefin coordination). Bond lengths are given in Å. Transition states are labeled TS.

in **I** (L = PH_3), and it is therefore qualitatively plausible that loss of phosphane is more facile for **II-1** than for **I-1** in the absence of any specific steric effects.

The incoming olefin can coordinate to **5** either *cis* or *trans* to the ancillary ligand L. We first consider *trans* coordination to **I-5** (see Figure 5). If the *x* and *y* axes are assigned to Ru=C and Ru–P, respectively, the LUMO of **I-5** is predominantly $d_{x^2-y^2}$ of the Ru atom, with a lobe at the empty coordination site (negative *y* axis), while the HOMOs correspond essentially to d_{yz} (HOMO) and d_{xz} (HOMO-1, only slightly below the HOMO). These orbitals are ideally oriented to interact with the frontier orbitals (π, π^*) of ethene in a *trans* approach ($\pi \rightarrow$ LUMO donation, HOMO $\rightarrow \pi^*$ or HOMO-1 $\rightarrow \pi^*$ backdonation). The *trans* coordination of ethene is thus electronically allowed. The energy decreases monotonically with decreasing Ru$\cdots$ethene distance in a series of constrained minimizations at various fixed Ru$\cdots$ethene separations. The *trans* addition of ethene to **I-5** is thus barrierless (unlike the addition to **I-1** in the associative mechanism). The resulting π complex **I-6** shows a perpendicular orientation of the ethene C=C bond relative to Ru=C (corresponding to HOMO $\rightarrow \pi^*$ backdonation), but the fact that internal rotation of the ethene moiety by 90° requires only 2.7 kcal mol^{-1} indicates that HOMO-1 $\rightarrow \pi^*$ backdonation is almost equally efficient. In the case of **II-5**, the electronic situation is qualitatively similar. The *trans* approach is again barrierless, and the most stable π complex **II-6** also shows a perpendicular orientation (see Figure 6), but there is a second local minimum **II-6a** which has an intermediate ethene twist angle and is 1 kcal mol^{-1} less stable than **II-6**. Compared with **I-6**, the Ru–C ethene bonds are more than 0.06 Å longer in **II-6**, which is in line with a weaker $C_2H_4 \rightarrow$ Ru donation due to a stronger *trans* influence of the Arduengo-type carbene ligand L in **II-6**. For the same reason the ethene binding energy is smaller in **II-6** (12.5 kcal mol^{-1}) than in **I-6** (14.1 kcal mol^{-1}).

The next reaction step is ring closure of the π complex **6** to give the ruthenacycle **7**. This involves the internal rotation of the ethene and methylidene ligands, opening of the Cl-Ru-Cl angle, and the formation of a new C–C bond (see Figure 5 and Figure 6). At the transition state **TS67** the internal rotations are so far advanced that the ruthenium and the three relevant carbon atoms approach coplanarity (C-Ru-C-C dihedral angle: 24° in **I**, 33° in **II**), and the Cl-Ru-Cl angle is nearly linear (172° in both cases), while the C–C distance for the bond to be formed is still quite large (2.37 Å in **I**, 2.53 Å in **II**). The calculated barriers ΔE_0 are 12.0 kcal mol^{-1} (**I**) and 6.3 kcal mol^{-1} (**II**). The resulting ruthenacycles **7** have very similar ring structures and Cl-Ru-Cl angles (177° in **I**, 180° in **II**), but show opposite relative stabilities. Energetically (in terms of ΔE_0), **I-7** lies 5.8 kcal mol^{-1} above **I-6**, whereas **II-7** is 3.4 kcal mol^{-1} below **II-6**. Since all species are sterically unencumbered, this difference must be related to the different electronic properties of the ancillary ligands. In a relative sense, the greater σ-donor strength of the Arduengo-type carbene ligand in **II** (compared to L = PH_3 in **I**) destabilizes the π complex **6** (see above), and also appears to stabilize the metallacycle **7**.

We now consider the overall energetics of the dissociative pathway with *trans* ethene coordination with focus on the ΔG°_{298} results (see Figure 9 and Figure 10). The initiation **1** $\rightarrow$ **5**

  0947-6539/02/0817-3969 $ 20.00+.50/0

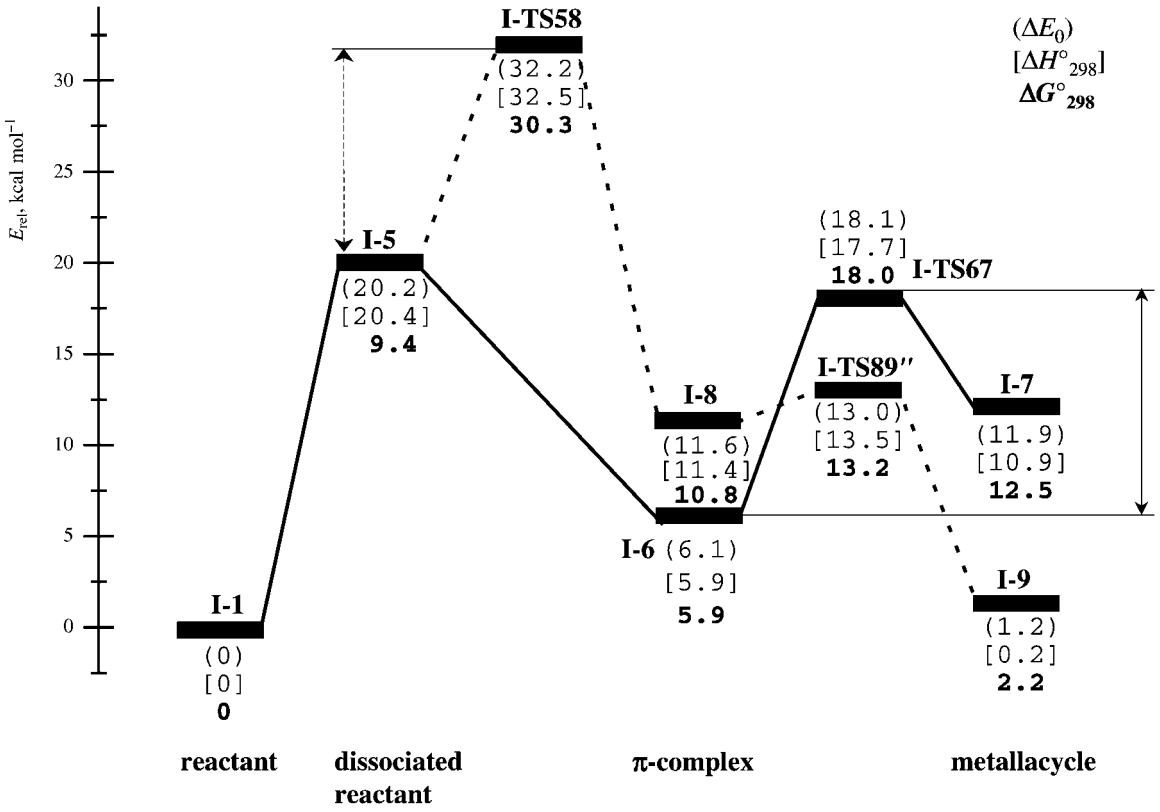

Figure 9. Potential energy profile of ethene metathesis for the dissociative mechanism with the $[(PH_3)_2Cl_2Ru{=}CH_2]$ catalyst (**I**). The notations are the same as in Figure 3. The dotted line corresponds to ethene attack in the position *cis* to the PH_3 ligand, and the solid line to *trans* attack. The arrows mark the rate-limiting steps in the catalytic cycle (**5**→**6**→**7**→**6**→**5**, **5**→**8**→**9**→**8**→**5**).

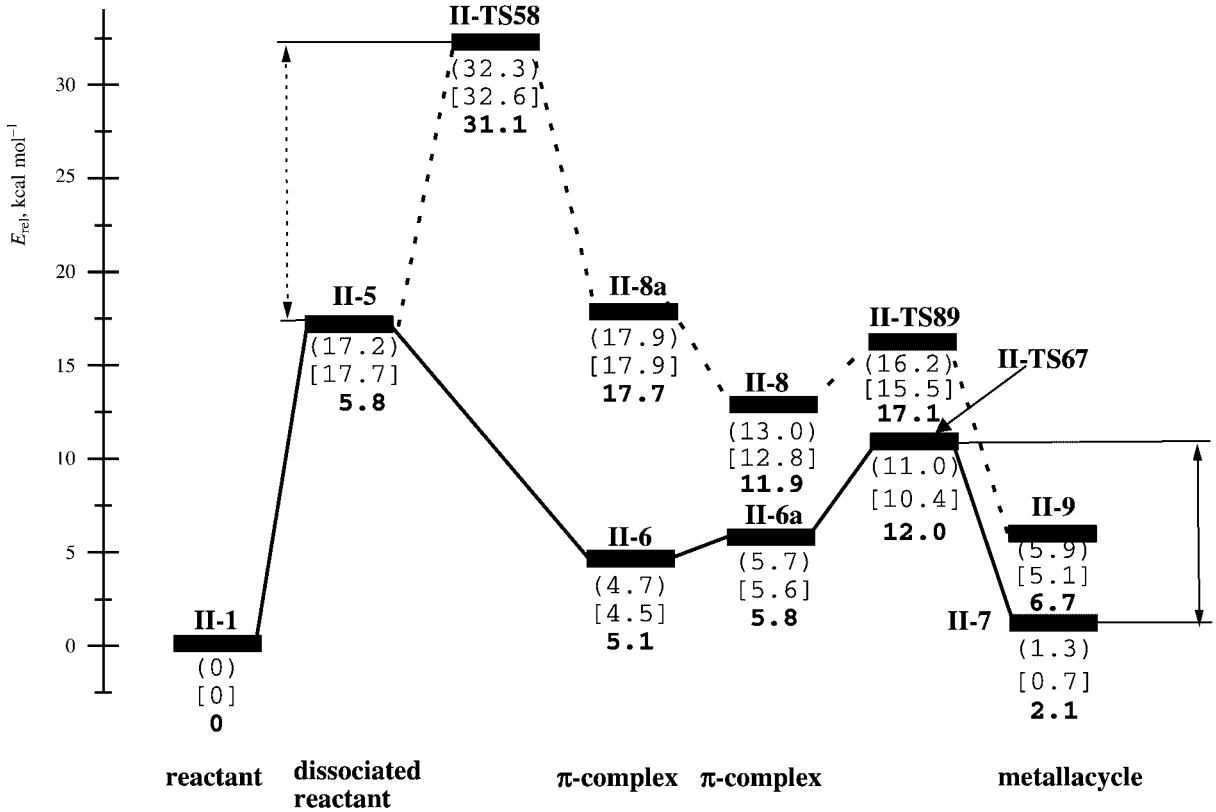

Figure 10. Potential energy profile of ethene metathesis for the dissociative mechanism with the $[(PH_3)(C_3N_2H_4)Cl_2Ru{=}CH_2]$ catalyst (**II**). The notations are the same as in Figure 3. The dotted line corresponds to ethene attack in the position *cis* to the imidazol-2-ylidene ligand, and the solid line to *trans* attack. The arrows mark the rate-limiting steps in the catalytic cycle (**5**→**6**→**7**→**6**→**5**, **5**→**8**→**9**→**8**→**5**).

0947-6539/02/0817-3970 $ 20.00+.50/0 *Chem. Eur. J.* **2002**, *8*, No. 17

by phosphane dissociation is more facile for **II** than for **I** (5.8 versus 9.4 kcal mol^{-1}). In the subsequent catalytic cycle for the degenerate metathesis (**5** → **6** → **7** → **6** → **5**), the maximum free-energy barrier for an elementary step is found for the ring closure **6** → **7** in the case of **I** (12.1 kcal mol^{-1}) and for the ring opening **7** → **6** in the case of **II** (9.9 kcal mol^{-1}). This suggests that **II** is a more active metathesis catalyst than **I** in the catalytic cycle.

An alternative reaction pathway after the initial loss of PH_3 involves olefin coordination to **5** in the position *cis* to the ancillary ligand between chlorine and methylidene (see Figure 7 and Figure 8). In the case of catalyst **I**, only one *cis* adduct **I-8** could be located on the potential energy surface; it resembles a distorted trigonal bipyramid (equatorial postions: CH_2, Cl, C_2H_4; axial positions: PH_3, Cl). In the corresponding transition state **I-TS58** the approaching ethene has already induced one of the chlorine atoms to move away from the basal plane towards the axial position (see Figure 7). This transition state is rather distorted, with a reorganization energy of 18.4 kcal mol^{-1} for the $(PH_3)Cl_2Ru{=}CH_2$ fragment, and is therefore associated with a high barrier ($\Delta E^{\neq}$ = 12.0 kcal mol^{-1}, $\Delta G^{\neq}_{298}$ = 20.9 kcal mol^{-1}). In the case of catalyst **II**, *cis* ethene attack occurs essentially in the basal plane (see **II-TS58**) and leads to a square-pyramidal *cis* adduct **II-8a** (basal ligands: CH_2, both Cl, C_2H_4), which can then rearrange to the more stable complex **II-8** with a distorted trigonal-bipyramidal structure that resembles **I-8** (see above). The transition state for ethene coordination (**II-TS58**) is sterically quite congested (e.g., Cl-Ru-Cl angle of 108.5° compared to 144.5° in **II-5**), and this again implies a high reorganization energy for the $(C_3N_2H_4)Cl_2Ru{=}CH_2$ fragment (14.4 kcal mol^{-1}) and high barriers ($\Delta E^{\neq}$ = 15.1 kcal mol^{-1}, $\Delta G^{\neq}_{298}$ = 25.3 kcal mol^{-1}). For both catalysts considered, *cis* ethene attack to give the active species **5** requires a large activation energy and is therefore not competitive with *trans* attack.

In contrast, the subsequent ring-closing reaction **8** → **9** is quite facile, with barriers of 2–5 kcal mol^{-1} for **I** and **II** and transition states that exhibit the expected features (see Figure 7 and Figure 8, distances of the forming C–C bonds in **TS89** of 2.4–2.5 Å). The ruthenacycle products **9** have qualitatively similar structures in which the two chlorine ligands are *cis* to each other. Relative to the isomeric ruthenacycles **7** with two *trans* chlorine ligands, the relative energies are calculated as **I-7** > **I-9** (ΔE_0 = 10.7 kcal mol^{-1}) and **II**-7 < **II-9** (ΔE_0 = −4.6 kcal mol^{-1}).

To summarize the results obtained so far, the dissociative mechanism with *trans* olefin coordination is clearly preferred. To assess the reliability of the BP86 results, we recalculated the key species on this pathway for catalyst **I**, using B3LYP geometry optimizations and CCSD(T) single-point calculations on BP86 geometries. The results are given in Table 1. The relative energies from the BP86 functional (used in the present study) and from the hybrid B3LYP functional are obviously close to each other (within 2 kcal mol^{-1}). The relative energies from the high-level ab initio CCSD(T) calculations tend to be slightly higher than the BP86 values (by 1.2–4.7 kcal mol^{-1}), but all three computational aproaches yield qualitatively the same energy profile. Hence, BP86 appears to be qualitatively reliable for the purposes of the present study.

Table 1. Relative energies[a] for catalyst **I**.

Species[b]	BP86	B3LYP	CCSD(T)//BP86[c]
I-1	0.0	0.0	0.0
I-5	22.3	20.3	25.9
I-6	6.1	7.7	7.3
I-TS67	18.8	18.3	20.8
I-7	10.7	11.5	15.4

[a] In kcal mol^{-1}, without corrections for zero-point vibrational energy. [b] Stationary points on the dissociative pathway with *trans* coordination of ethene. [c] CCSD(T) single-point calculation on BP86 geometries.

Calculations on $[(PMe_3)_2Cl_2Ru{=}CH_2]$: The real-life metathesis catalysts contain bulky trialkylphosphanes such as PCy_3, which are stronger σ donors but are also sterically much more demanding than the PH_3 ligand used in our model studies. We replaced PH_3 in **I** by PMe_3 to give catalyst **III** and examined the electronic effects caused by a stronger σ donor without introducing significant steric congestion.

Calculations were performed only for the dissociative pathway with *trans* coordination of the incoming olefin. The reactions are analogous to those for the unsubstituted catalyst **I**, and the geometries of the stationary points are very similar to those in Figure 5 and hence not shown. The resulting reaction profile is given in Figure 11 and compared with that of the unsubstituted catalyst **I**. The two profiles are qualitatively similar, with a shift towards higher relative energies upon substitution.

The initial dissociation **1** → **5** is more endothermic for PMe_3 (ΔE_0 = 26.6 kcal mol^{-1}) than for PH_3 (ΔE_0 = 20.2 kcal mol^{-1}), which reflects an increase of the Ru–P bond energy with increasing σ-donor strength of the phosphane ligand (in the absence of adverse steric effects). The subsequent *trans* coordination of ethene **5** → **6** is less exothermic for PMe_3 (ΔE_0 = −10.9 kcal mol^{-1}) than PH_3 (ΔE_0 = −14.1 kcal mol^{-1}) due to the stronger *trans* influence of the PMe_3 ligand. This destabilization of the π complex leads to a smaller barrier for ring closure **6** → **7** (i.e., 9.9 vs 12.0 kcal mol^{-1} in terms of ΔE_0), since the essentially σ-bound transition state **TS67** is less affected by the *trans* influence of the phosphane ligand. Considering the calculated Gibbs free energies ΔG°_{298}, the formation of the π complex **5** → **6** is still slighty exoergic for PH_3 (−3.5 kcal mol^{-1}) but nearly isoergic for PMe_3 (+0.3 kcal mol^{-1}), and ring closure remains the rate-limiting step in the catalytic cycle (**5** → **6** → **7** → **6** → **5**), with a slightly smaller barrier for PMe_3 (9.6 vs 12.1 kcal mol^{-1} in terms of $\Delta G^{\neq}_{298}$). The replacement of PH_3 by PMe_3 in catalyst **I** is thus expected to increase its activity in the catalytic cycle (**5** → **6** → **7** → **6** → **5**) while making the initiation (**1** → **5**) more difficult. It should be stressed, however, that these results cannot be generalized to bulkier phosphanes without taking steric effects into account.

Comparison with previous calculations: Car–Parrinello molecular dynamics (MD) simulations have been performed[30] to study the behavior of the catalyst $[(PH_3)_2Cl_2Ru{=}CH_2]$ (**I-1**) and its reactions with ethene at several temperatures between

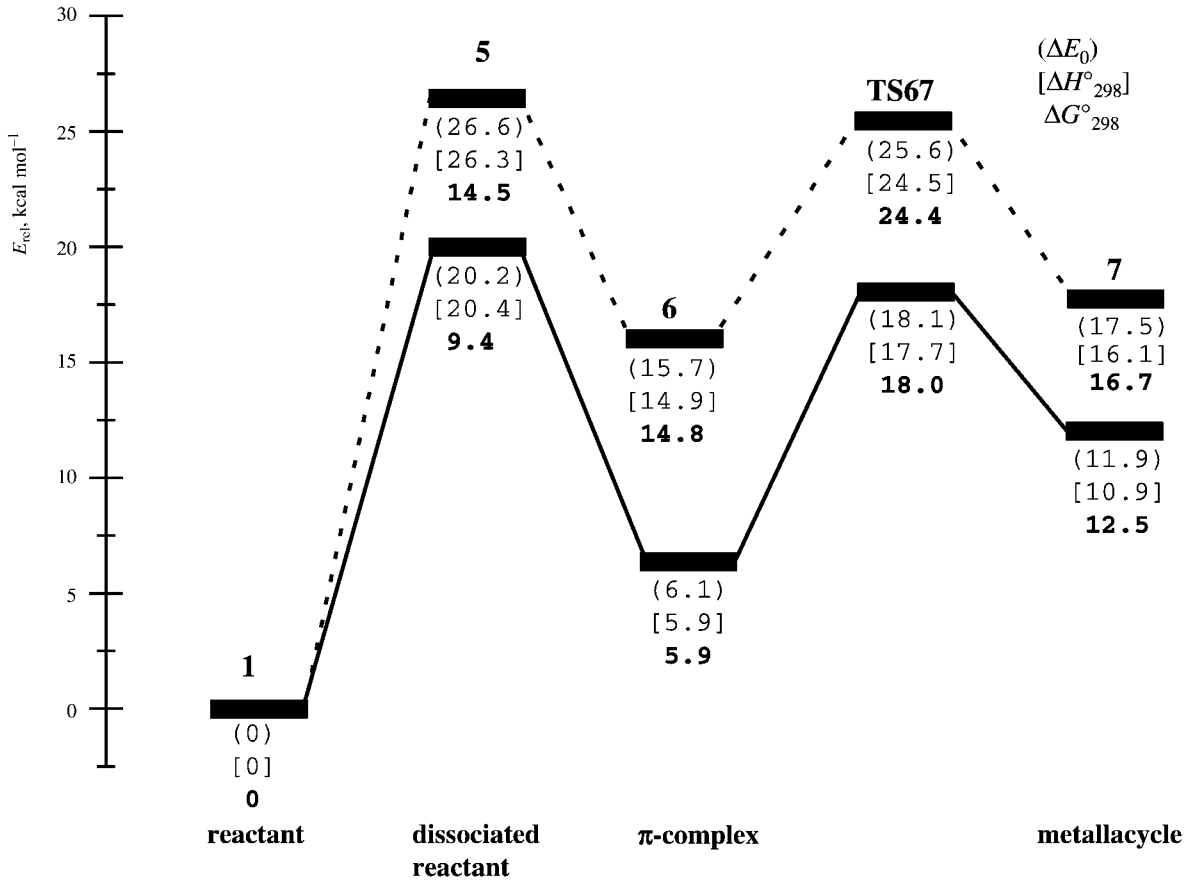

Figure 11. Comparison of the potential energy profiles for the dissociative mechanism (*trans* attack) with the $[(PH_3)_2Cl_2Ru{=}CH_2]$ catalyst (**I**, solid line) and the $[(PMe_3)_2Cl_2Ru{=}CH_2]$ catalyst (**III**, dotted line).

300 K and 1273 K. This work emphasized the identification of dynamic and reactive events to gain qualitative mechanistic insights, and consequently the MD simulations were run with considerable amounts of internal energy, particularly when starting from shortened Ru–P bonds to provide selective bond activation.[30] In constrast, our work aims at finding all relevant stationary points along the minimum-energy paths of different conceivable mechanisms to characterize the underlying potential energy surface in more quantitative detail. The two studies employ the same density functional (BP86) and should thus complement each other.

To be more specific, both studies find rather "soft" Cl-Ru-Cl angles (*cis*/*trans* isomerization in MD, values between 90° and 180° encountered in various optimized structures) and relatively facile phosphane dissociation (seen in MD at 1273 K, low $\Delta G^{\ddagger}_{298}$ value of 9.4 kcal mol^{-1}). Internal rotation of the methylidene ligand in **I-1** and **I-5** is observed during the MD runs and associated with moderate barriers in our calculations ($\Delta E_o = 12.1$ and 20.5 kcal mol^{-1}, respectively).

However, there are also more pronounced differences. In the case of the associative mechanism, the MD study[30] shows the incoming ethene approaching the catalyst **I-1** with the C=C bond parallel to the equatorial plane. In our calculations (see Figure 1) this approach is unfavorable since it proceeds through a second-order saddle point which lies several kcal mol^{-1} above the "perpendicular" transition state **I-TS12** (apparently missed in MD). Moreover, our calculations suggest a complicated sequence of conformational changes for the ethene and methylidene ligands along the associative minimum-energy path (see Figure 1) which are not mentioned in the MD work.[30] Concerning the dissociative mechanism, the MD runs apparently assumed a *cis* ethene attack to give the active monophosphane species **I-5** (see Figure 5 of ref. [30a]) which led to a direct metathesis reaction. In our calculations, this path was also found (see Figure 7), but the alternative *trans* attack is much more preferred (see Figure 5 and Figure 9). The MD study does not mention this alternative, nor does it address the π complexes that occur as intermediates (see Figures 1–11). Hence, the present calculations have revealed many mechanistic features not yet probed by MD,[30] and may therefore serve as starting point for future MD work.

Discussion

In the present density functional study we have examined possible mechanisms for metathesis reactions involving ethene and model catalysts, in particular $[(PH_3)_2Cl_2Ru{=}CH_2]$ (**I**) and $[(PH_3)(C_3N_2H_4)Cl_2Ru{=}CH_2]$ (**II**). The associative pathway requires initial ethene coordination to form a π complex followed by migratory insertion to give a ruthenacyclobutane. For both catalysts, the initial olefin coordination exhibits a high barrier ($\Delta G^{\ddagger}_{298} \approx 22-25$ kcal mol^{-1}) and is the

  0947-6539/02/0817-3972 $ 20.00+.50/0 *Chem. Eur. J.* **2002**, *8*, No. 17

rate-determining step. The dissociative pathway starts with the dissociation of a phosphane ligand, which is calculated to be rather facile ($\Delta G^{\ddagger}_{298} \approx 5-10$ kcal mol^{-1}). The resulting tetracoordinate active species [(L)Cl_2Ru=CH_2] can coordinate ethene in *cis* or *trans* position to the ligand L. The *cis* attack is quite unfavorable, with coordination barriers of $\Delta G^{\ddagger}_{298} \approx 22-25$ kcal mol^{-1}, and is therefore not relevant for the mechanism under study. In contrast, *trans* coordination is barrierless. Thus, the rearrangement between the *trans* adduct and the ruthenacyclobutane represents the rate-determining step in the catalytic cycle ($\Delta G^{\ddagger}_{298} \approx 10-12$ kcal mol^{-1}).

The Gibbs free energy changes given above contain entropic contributions which generally increase the barriers for addition reactions and decrease dissociation energies due to the changing number of particles. In the gas phase at 298 K these entropic contributions are calculated to be on the order of 10 kcal mol^{-1} both for associative and dissociative processes (see reactions **1** → **2**, **1** → **5**, **5** → **6**, **5** → **8** in Figure 1, Figure 2, Figure 9, and Figure 10). In solution, these entropic effects are expected to be smaller because of concomitant solvent reorganization, and experimental values of around 4 kcal mol^{-1} have recently been reported for phosphane dissociation **1** → **5** from a series of ruthenium complexes in [D_8]toluene.[17] Even when such reduced entropic contributions in solution are taken into account, the dissociative mechanism remains slightly favored over the associative mechanism for our model catalysts. On the dissociative pathway, the preference for *trans* rather than *cis* olefin coordination arises from energetic reasons and does not depend on entropic arguments. However, the entropic contributions do affect the relative ease of the various steps on the preferred pathway: the initial dissociation **1** → **5** is most costly in terms of $\Delta H^{\ddagger}_{298}$, but not in terms of $\Delta G^{\ddagger}_{298}$ (see Figure 9 and Figure 10).

In summary, the calculations on the model catalysts favor the dissociative mechanism with *trans* olefin coordination. This pathway is sterically less demanding than the alternatives considered (see above) and should therefore be even more preferred for real-life metathesis catalysts with bulky substituents.

We now relate our theoretical results for the dissociative mechanism to the experimental evidence from recent kinetic studies in solution,[17] which have adressed the exchange of free and bound phosphane in a series of 14 ruthenium complexes [(PR_3)(L)X_2Ru=CHR′] for various combinations of ligands (typically R = Cy; L = PR_3, NHC; X = Cl, Br, I; R′ = H, Ph). The measured activation enthalpies correspond to phosphane dissociation enthalpies and range from 19 to 27 kcal mol^{-1}.[17] The calculated ΔH°_{298} values for our model catalysts [(PH_3)$_2$$Cl_2$Ru=$CH_2$], [($PH_3$)($C_3N_2H_4$)$Cl_2$Ru=$CH_2$], and [($PMe_3$)$_2$$Cl_2$Ru=$CH_2$] are 20.4, 17.7, and 26.3 kcal mol^{-1}, respectively (see Figure 9, Figure 10, and Figure 11). The closest analogues from the experimental study are [(PCy_3)$_2$$Cl_2$Ru=CHPh] and [($PCy_3$)(Imes)$Cl_2$Ru=CHPh] (Imes = 2,5-dimesitylimidazol-2-ylidene), with ΔH values of 23 ± 0.5 and 25 ± 4 kcal mol^{-1}, respectively.[17] The theoretical and experimental results cannot be compared directly (different ligands), but they are at least of similar magnitude. Closer analysis indicates that the calculated ΔH values are probably somewhat underestimated (consistent with the expectations from the more accurate CCSD(T) calculations, see Table 1). Experimentally, the studied catalysts with R′ = H are not active,[17] and our calculations show that the replacement of R′ = H by R′ = Ph indeed facilitates phosphane dissociation by 2–3 kcal mol^{-1} (resulting, e.g., in $\Delta H^{\circ}_{298} = 17.8$ kcal mol^{-1} for [(PH_3)$_2$$Cl_2$Ru=CHPh], which lies below the observed range). More disturbing are trends in ΔH that are observed when replacing a trialkylphosphane ligand by an N-heterocyclic carbene. Experimentally, this leads to much slower phosphane dissociation and hence higher ΔH values[17] (e.g., in [(PCy_3)(L)Cl_2Ru=CHPh], see above), whereas the opposite trend is predicted theoretically for our model catalysts [(PH_3)(L)Cl_2Ru=CH_2] (L = PH_3 versus L = $C_3N_2H_4$, see above). The theoretical result is qualitatively plausible, since electronic effects should favor the dissociation of a phosphane ligand *trans* to the stronger σ donor (NHC). The contrary experimental finding must therefore be due to steric effects[31] exerted by the bulky phosphane substituents. This emphasizes the need for theoretical studies on the real catalysts,[31] especially when there may be counteracting electronic and steric effects.

It is experimentally well established[3, 4, 17] that introducing N-heterocyclic carbene ligands considerably improves the catalytic activity for olefin metathesis. Within the framework of the dissociative mechanism with *trans* olefin coordination, this must be reflected in the catalytic cycle **5** → **6** → **7** → **6** → **5** (see Figure 9, Figure 10, and Figure 11). The variation of the ligand L in (L)Cl_2Ru=CH_2 (**5**) can indeed tune the relative energies of the other relevant species (**6**, **TS67**, **7**). Focusing on the Gibbs free energies ΔG°_{298}, the π complex **6** is more stable than the metallacycle **7** for L = PH_3 (by 6.6 kcal mol^{-1}), but less stable for L = $C_3N_2H_4$ (by 3.0 kcal mol^{-1}). Consequently, the rate-determining step on the ΔG° surface also depends on L and corresponds to ring closure **6** → **7** in the first case and to ring opening **7** → **6** in the second. The respective barriers ($\Delta G^{\ddagger}_{298}$) are 12.1 kcal mol^{-1} for L = PH_3 and 9.9 kcal mol^{-1} for L = $C_3N_2H_4$, which is consistent with the observed greater activity of metathesis catalysts containing an NHC ligand.[3, 4, 17] One should be cautious, however, about drawing more general conclusions: for example, in the case of L = PMe_3, **6** and **7** are close in energy, and the rate-limiting barrier is similar to that for L = $C_3N_2H_4$. It would therefore seem advisable to study more ligands L in order to better understand the electronic and steric effects that govern the catalytic activity. For our present ligands (L = PH_3, PMe_3, $C_3N_2H_4$), the changes in the calculated relative energies can at least partly be rationalized in terms of σ-donor strengths (see above). Finally, note that the active species **5** is rather stable on the calculated ΔG° surface due to large entropic contributions (gas-phase values), but less so on the ΔE surface, where it even lies above **TS67** (see Figures 9, Figure 10, and Figure 11). Given the smaller entropic contributions that may be more appropriate in solution (see above), it seems unlikely that the dissociation of the π complex **6** → **5** could become the rate-determining step. However, this possibility cannot be ruled out and may need to be considered for other ligands L.

In the dissociative mechanism, the tetracoordinate active species **5** may recombine with free phosphane to regenerate the initial catalyst **1** (at a rate proportional to k_{-1}) or it can

bind olefin substrate and undergo productive olefin metathesis reactions (at a rate proportional to k_2). In recent kinetic work,[17] the k_{-1}/k_2 ratio has been measured in solution for eight ruthenium complexes $[(PR_3)(L)X_2Ru{=}CHR']$ with different combinations of ligands, by monitoring the ^1H NMR signal of the starting alkylidene as a function of time. The observed k_{-1}/k_2 ratios are generally much higher for $L = PR_3$ than for L = NHC, typically by four orders of magnitude.[17] These results have been discussed in terms of the competition between phosphane recoordination and olefin binding to **5** assuming "that all of the steps after olefin coordination (particularly metallacyclobutane formation) are fast".[17] According to our current DFT results for isolated model catalysts $[(PR_3)(L)Cl_2Ru{=}CH_2]$, this assumption holds only for the *cis* attack of ethene, but not for the preferred *trans* attack (see ΔG° values in Figure 9 and Figure 10). In the latter case, olefin coordination is calculated to be barrierless, and the rate-determining step on the ΔG° surface involves the metallacyclobutane (see above). This suggests associating the rate constant k_2 with metallacycle formation (leading to the disappearance of the monitored ^1H NMR signal): the calculated barriers on the ΔG° surface then imply $k_2(L = NHC) > k_2(L = PH_3)$, which would be consistent with the observed trends in the k_{-1}/k_2 ratios.[17] Our gas-phase model calculations thus raise the possibility of a different interpretation of the experimental data on k_{-1}/k_2. Note, however, that the kinetic measurements were carried out in solution with catalysts having much bulkier substituents.[17] Therefore, the experimental k_{-1}/k_2 ratios will be affected by solvent reorganization and steric effects, which are not included in the calculations.

Conclusion

Using density functional calculations we have identified associative and dissociative pathways for olefin metathesis reactions involving ethene and model ruthenium-based catalysts $[(PR_3)(L)Cl_2Ru{=}CH_2]$. Both π complexes and ruthenacyclobutanes appear as intermediates on these pathways. The dissociative mechanism with *trans* olefin coordination is favored over the other alternatives. It proceeds by a facile dissociation of PR_3 followed by a barrierless coordination of ethene *trans* to L and rearrangement of the resulting π complex to give the ruthenacycle by migratory insertion (plus the reverse reactions in the case of degenerate metathesis). Our model study emphasizes the electronic effects exerted by the ligands. For a given phosphane PR_3, an increasing σ-donor ability of L facilitates the initial dissociation of PR_3 and destabilizes the intermediate π complex, which makes the insertion more favorable. Electronically, the most efficient catalysts are expected to contain one weak and one strong σ-donor ancillary ligand to promote dissociation and insertion, respectively. Steric effects are not important in our model systems, but need to be considered in the real catalysts employed experimentally, which contain much bulkier ligands.

Acknowledgement

We are grateful to Prof. A. Fürstner for attracting our attention to this field. We thank him as well as Prof. P. Chen, Dr. K. Angermund, and Dr. C. Adlhart for valuable discussions.

[1] K. J. Ivin, J. C. Mol, *Olefin Metathesis and Metathesis Polymerization*, Academic Press, San Diego, **1997**.
[2] F. Zaragoza Dörwald, *Metal Carbenes in Organic Synthesis*, Wiley-VCH, Weinheim, **1999**.
[3] A. Fürstner, *Angew. Chem.* **2000**, *112*, 3140 – 3172; *Angew. Chem. Int. Ed.* **2000**, *39*, 3012 – 3043.
[4] T. M. Trnka, R. H. Grubbs, *Acc. Chem. Res.* **2001**, *34*, 18 – 29.
[5] S. T. Nguyen, L. K. Johnson, R. H. Grubbs, J. W. Ziller, *J. Am. Chem. Soc.* **1992**, *114*, 3974 – 3975.
[6] P. Schwab, R. H. Grubbs, J. W. Ziller, *J. Am. Chem. Soc.* **1996**, *118*, 100 – 110.
[7] Reviews on NHC: a) W. A. Herrmann, C. Köcher, *Angew. Chem.* **1997**, *109*, 2256 – 2282; *Angew. Chem. Int. Ed.* **1997**, *36*, 2162 – 2187; b) A. J. Arduengo, *Acc. Chem. Res.* **1999**, *32*, 913 – 921.
[8] a) M. Scholl, T. M. Trnka, J. P. Morgan, R. H. Grubbs, *Tetrahedron Lett.* **1999**, *40*, 2247 – 2250; b) M. Scholl, S. Ding, W. C. Lee, R. H. Grubbs, *Org. Lett.* **1999**, *1*, 953 – 956.
[9] a) J. Huang, E. D. Stevens, S. P. Nolan, J. L. Petersen, *J. Am. Chem. Soc.* **1999**, *121*, 2674 – 2678; b) J. Huang, H.-J. Schanz, S. P. Nolan, *Organometallics* **1999**, *18*, 5375 – 5380.
[10] a) T. Weskamp, F. J. Kohl, W. Hieringer, D. Gleich, W. A. Herrmann, *Angew. Chem.* **1999**, *111*, 2573 – 2576; *Angew. Chem. Int. Ed.* **1999**, *38*, 2416 – 2419; b) L. Ackermann, A. Fürstner, T. Weskamp, F. J. Kohl, W. A. Herrmann, *Tetrahedron Lett.* **1999**, *40*, 4787 – 4790; c) T. Weskamp, F. J. Kohl, W. A. Herrmann, *J. Organomet. Chem.* **1999**, *582*, 362 – 365.
[11] a) S. M. Hansen, F. Rominger, M. Metz, P. Hofmann, *Chem. Eur. J.* **1999**, *5*, 557 – 566; b) S. M. Hansen, M. A. O. Volland, F. Rominger, F. Eisenträger, P. Hofmann, *Angew. Chem.* **1999**, *111*, 1360 – 1364; *Angew. Chem. Int. Ed.* **1999**, *38*, 1273 – 1276; c) P. Hofmann, M. A. O. Volland, S. M. Hansen, F. Eisenträger, J. H. Gross, K. Stengel, *J. Organomet. Chem.* **2000**, *606*, 88 – 92.
[12] J.-L. Hérisson, Y. Chauvin, *Makromol. Chem.* **1970**, *141*, 161 – 176.
[13] E. L. Dias, S. T. Nguyen, R. H. Grubbs, *J. Am. Chem. Soc.* **1997**, *119*, 3887 – 3897.
[14] M. Ulman, R. H. Grubbs, *Organometallics* **1998**, *17*, 2484 – 2489.
[15] M. Ulman, R. H. Grubbs, *J. Org. Chem.* **1999**, *64*, 7202 – 7207.
[16] M. S. Sanford, M. Ulman, R. H. Grubbs, *J. Am. Chem. Soc.* **2001**, *123*, 749 – 750.
[17] M. S. Sanford, J. A. Love, R. H. Grubbs, *J. Am. Chem. Soc.* **2001**, *123*, 6543 – 6554.
[18] C. Hinderling, C. Adlhart, P. Chen, *Angew. Chem.* **1998**, *110*, 2831 – 2835; *Angew. Chem. Int. Ed.* **1998**, 37, 2685 – 2689.
[19] C. Adlhart, C. Hinderling, H. Baumann, P. Chen, *J. Am. Chem. Soc.* **2000**, *122*, 8204 – 8214.
[20] C. Adlhart, M. A. O. Volland, P. Hofmann, P. Chen, *Helv. Chim. Acta* **2000**, 83, 3306 – 3311.
[21] M. A. O. Volland, C. Adlhart, C. A. Kiener, P. Chen, P. Hofmann, *Chem. Eur. J.* **2001**, *7*, 4621 – 4632.
[22] J. A. Tallarico, P. J. Bonitatebus, Jr., M. L. Snapper, *J. Am. Chem. Soc.* **1997**, *119*, 7157 – 7158.
[23] M. S. Sanford, L. M. Henling, M. W. Day, R. H. Grubbs, *Angew. Chem.* **2000**, *112*, 3593 – 3595; *Angew. Chem. Int. Ed.* **2000**, *39*, 3451 – 3453.
[24] M. T. Reetz, M. H. Becker, M. Liebl, A. Fürstner, *Angew. Chem.* **2000**, *112*, 1294 – 1298; *Angew. Chem. Int. Ed.* **2000**, *39*, 1236 – 1239.
[25] A. Fürstner, L. Ackermann, B. Gabor, R.Goddard, C. W. Lehmann, R. Mynott, F. Stelzer, O. R. Thiel, *Chem. Eur. J.* **2001**, *7*, 3236 – 3253.
[26] a) O. Eisenstein, R. Hoffmann, A. R. Rossi, *J. Am. Chem. Soc.* **1981**, *103*, 5582 – 5584; b) A. K. Rappé, T. H. Upton, *Organometallics* **1984**, *3*, 1440 – 1442; c) T. H. Upton, A. K. Rappé, *J. Am. Chem. Soc.* **1985**, *107*, 1206 – 1218.
[27] T. R. Cundari, M. S. Gordon, *Organometallics* **1992**, *11*, 55 – 63.
[28] E. Folga, T. Ziegler, *Organometallics* **1993**, *12*, 325 – 337.

  0947-6539/02/0817-3974 $ 20.00+.50/0

[29] Y.-D. Wu, Z.-H. Peng, *J. Am. Chem. Soc.* **1997**, *119*, 8043–8049.
[30] a) O. M. Aagaard, R. J. Meier, F. Buda, *J. Am. Chem. Soc.* **1998**, *120*, 7174–7182; b) R. J. Meier, O. M. Aagaard, F. Buda, *J. Mol. Catal. A* **2000**, *160*, 189–197.
[31] a) C. Adlhart, P. Chen, personal communication, December **2001**; b) C. Adlhart, P. Chen, Heidelberg Forum of Molecular Catalysis, Poster 12, Heidelberg, December 7th, **2001**.
[32] a) A. Fürstner, O. R. Thiel, G. Blanda, *Org. Lett.* **2000**, *2*, 3731; b) A. Fürstner, T. Dierkes, O. R. Thiel, G. Blanda, *Chem. Eur. J.* **2001**, *7*, 5286–5298.
[33] R. G. Parr, W. Yang, *Density Functional Theory of Atoms and Molecules*, Oxford University Press, New York, **1989**.
[34] W. Koch, M. C. Holthausen, *A Chemist's Guide to Density Functional Theory*, Wiley-VCH, Weinheim, **2000**.
[35] A. D. Becke, *Phys. Rev. A* **1988**, *38*, 3098–3100.
[36] J. P. Perdew, *Phys. Rev. B* **1986**, *33*, 8822–8824.
[37] D. Andrae, U. Häussermann, M. Dolg, H. Stoll, *Theor. Chim. Acta* **1990**, *77*, 123–141.
[38] a) W. J. Hehre, R. Ditchfield, J. A. Pople, *J. Chem. Phys.* **1972**, *56*, 2257; b) P. C. Hariharan, J. A. Pople, *Theor. Chim. Acta* **1973**, 28, 213; c) M. M. Francl, W. J. Pietro, W. J. Hehre, J. S. Binkley, M. S. Gordon, D. J. DeFrees, J. A. Pople, *J. Chem. Phys.* **1982**, *77*, 3654–3665.
[39] a) R. Ahlrichs, M. Bär, M. Häser, H. Horn, C. M. Kölmel, *Chem. Phys. Lett.* **1989**, *162*, 165–169; b) O. Treutler, R. Ahlrichs, *J. Chem. Phys.* **1995**, *102*, 346–354; c) K. Eichkorn, O. Treutler, H. Öhm, M. Häser, R. Ahlrichs, *Chem. Phys. Lett.* **1995**, *242*, 652–660.
[40] K. Eichkorn, O. Treutler, H. Öhm, M. Häser, R. Ahlrichs, *Chem. Phys. Lett.* **1995**, *240*, 283–289.
[41] Gaussian 98 (Revision A.9) M. J. Frisch, G. W. Trucks, H. B. Schlegel, G. E. Scuseria, M. A. Robb, J. R. Cheeseman, V. G. Zakrzewski, J. A. Montgomery, Jr., R. E. Stratmann, J. C. Burant, S. Dapprich, J. M. Millam, A. D. Daniels, K. N. Kudin, M. C. Strain, O. Farkas, J. Tomasi, V.Barone, M. Cossi, R. Cammi, B. Mennucci, C. Pomelli, C. Adamo, S.Clifford, J. Ochterski, G. A. Petersson, P. Y. Ayala, Q. Cui, K.Morokuma, D. K. Malick, A. D. Rabuck, K. Raghavachari, J. B. Foresman, J. Cioslowski, J. V. Ortiz, A. G. Baboul, B. B. Stefanov, G. Liu, A. Liashenko, P. Piskorz, I. Komaromi, R.Gomperts, R. L. Martin, D. J. Fox, T. Keith, M. A. Al-Laham, C. Y. Peng, A. Nanayakkara, C. Gonzalez, M. Challacombe, P. M. W. Gill, B. Johnson, W. Chen, M. W. Wong, J. L. Andres, C.Gonzalez, M. Head-Gordon, E. S. Replogle, J. A. Pople, Gaussian, Inc., Pittsburgh, PA, **1998**.
[42] T. Ziegler, *Chem. Rev.* **1991**, *91*, 651–667.
[43] T. Ziegler, *Can. J.Chem.* **1995**, *73*, 743–761.
[44] V. Jonas, W. Thiel, *J. Chem. Phys.* **1995**, *102*, 8474–8484.
[45] Special issue on computational transition metal chemistry: *Chem. Rev.* **2000**, *100*, 351–818.
[46] A. D. Becke, *J. Chem. Phys.* **1993**, *98*, 5648–5652.
[47] P. J. Stevens, F. J. Devlin, C. F. Chabalowski, M. J. Frisch, *J. Phys. Chem.* **1994**, *98*, 11623–11627.
[48] G. D. Purvis III, R. J. Bartlett, *J. Chem. Phys.* **1982**, *76*, 1910–1918.
[49] K. Raghavachari, G. W. Trucks, J. A. Pople, M. Head-Gordon, *Chem. Phys. Lett.* **1989**, *157*, 479–483.
[50] MOLPRO, a package of ab initio programs designed by H.-J. Werner and P. J. Knowles, version 2000.1, R. D. Amos, A. Bernhardsson, A. Berning, P. Celani, D. L. Cooper, M. J. O. Deegan, A. J. Dobbyn, F. Eckert, C. Hampel, G. Hetzer, P. J. Knowles, T. Korona, R. Lindh, A. W. Lloyd, S. J. McNicholas, F. R. Manby, W. Meyer, M. E. Mura, A. Nicklass, P. Palmieri, R. Pitzer, G. Rauhut, M. Schütz, U. Schumann, H. Stoll, A. J. Stone, R. Tarroni, T. Thorsteinsson, and H.-J. Werner, University of Birmingham, **2000**.

Received: February 28, 2002 [F3909]